ELECTRON SPECTROSCOPY STUDIES OF VACUUM DEPOSITED CHROMIUM AND COBALT LAYERS

Jani Sainio

Laboratory of Physics
Helsinki University of Technology
Espoo, Finland

Dissertation for the degree of Doctor of Science in Technology to be presented with due permission of the Department of Engineering Physics and Mathematics for public examination and debate in Auditorium L at Helsinki University of Technology (Espoo, Finland) on the 8th of December, 2005, at 13 o'clock.

Dissertations of Laboratory of Physics, Helsinki University of Technology
ISSN 1455-1802

Dissertation 136 (2005):
Jani Sainio: Electron spectroscopy studies of vacuum deposited chromium and cobalt layers
ISBN 951-22-7879-0 (print)
ISBN 951-22-7880-4 (electronic)

Otamedia OY
ESPOO 2005

Abstract

Vacuum created model systems give the possibility for detailed study of the substrate–adsorbate interaction. In this work two systems have been created by vacuum deposition and these have been characterized with different electron spectroscopies. A chromium oxide model catalyst has been studied with X-ray photoelectron spectroscopy (XPS) and a magnetically interesting epitaxial Co/Cu system has been characterized with low energy electron diffraction (LEED).

Alumina supported chromium oxides are widely used as dehydrogenation catalysts. The nature of the active sites and the reaction paths are still somewhat unclear. We have used the model catalyst approach in order to understand the properties of supported chromium oxide catalysts. The growth of chromium on a thin alumina film has been studied. The oxidation and reduction of this model catalyst and alumina supported chromium oxide catalysts have been compared. The model catalyst can be oxidized under vacuum to the active oxidation state Cr^{3+}, but not further. In calcination and reduction the model catalyst was found to exhibit similar behavior as supported catalyst. This similarity suggests that the model catalyst can be used to study e.g. dehydrogenation reactions carried out on supported chromium oxides despite of the structural differences.

The chemical state information obtained from XPS measurements by peak fitting is subject to many systematic and random errors. We have studied the effect of the background subtraction method on the derived chemical state proportions of chromium and iron oxides with two oxidation states. The effect of the background choice was found to be comparable to typical systematic errors related to uncertain peak fitting parameters.

Epitaxial layers of Co and Cu show interesting magnetic properties, such as giant magnetoresistance. Undesired interface mixing has been observed when growing these layers. In this work Co was deposited onto a Cu(001) single crystal to model the interface structure. Co was found to form random surface alloys exhibiting substitutional copper sites. When the Co coverage increases to several monolayers, a transition to layer growth is observed. These findings can be used to model the magnetic properties of Co/Cu layers.

Preface

This thesis has been prepared in the Laboratory of Physics at Helsinki University of Technology during the years 2001–2005. I would like to thank Professor Pekka Hautojärvi for giving me the opportunity to work in the Surface Science group.

I wish to express my gratitude to Docent Jouko Lahtinen for his expert guidance and invaluable help whenever I've encountered problems in this research. I also wish to thank all of my collaborators from the Laboratory of Physics, the Department of Chemical Technology and from Dublin City University.

In addition, I want to thank all of the people in the Laboratory, especially in the Surface Science group, for providing an enthusiastic working environment. A very special thanks belongs to former and current lunch group members Mikko Aronniemi, Jukka Katainen, Matti Paajanen and Lauri Salminen. All of the help from the technical and administrative staff is also greatly appreciated.

Finally, I want to thank my family and friends for their support and for coming up with all of the much needed free time activities to balance out long working hours.

Helsinki, 2005

Jani Sainio

Contents

List of publications

This thesis consists of an overview and the following publications:

I M. Eriksson, J. Sainio, and J. Lahtinen, *Chromium deposition on ordered alumina films: An x-ray photoelectron spectroscopy study of the interaction with oxygen*, Journal of Chemical Physics **116**, 3870-3874 (2002).

II J. Sainio, M. Eriksson, and J. Lahtinen, *Interaction of oxygen with chromium deposited on Al_2O_3/NiAl(110)*, Surface Science **532-535**, 396-401 (2003).

III S. Airaksinen, O. Krause, J. Sainio, J. Lahtinen, K.-j. Chao, O. Guerrero-Peréz, and M. Bañares, *Reduction of chromia/alumina catalyst monitored by DRIFTS-mass spectrometry and TPR-Raman spectroscopy*, Physical Chemistry Chemical Physics **5**, 4371-4377 (2003).

IV J. Sainio, M. Aronniemi, O. Pakarinen, K. Kauraala, S. Airaksinen, O. Krause, and J. Lahtinen, *An XPS study of CrO_x on a thin alumina film and in alumina supported catalysts*, Applied Surface Science **252**, 1076-1083 (2005)

V M. Aronniemi, J. Sainio, and J. Lahtinen, *Chemical state quantification of iron and chromium oxides using XPS: the effect of the background subtraction method*, Surface Science **578**, 108-123 (2005).

VI J. Sainio, E. AlShamaileh, J. Lahtinen, and C. Barnes, *Initial growth of Co on Cu(001) studied with LEED I(V)*, Surface Review and Letters **10**, 641-648 (2003).

The roman numerals are used in this overview when referring to the publications.

The author has had an active role in all stages of the research reported in this work. He has written publications II, IV and VI. He has contributed actively in the experiments, analysis and writing of publications I and V. The author is responsible for the XPS related work in publication III.

Chapter 1

Introduction

Surface science has given important insight into catalysis and materials science over the last decades. Traditional surface science is involved in studies of single crystals and adsorption of gases or metallic adsorbates on them. These are usually related to catalytic surface reactions or otherwise interesting electronic or magnetic properties.

To be able to study the absorbate–substrate interaction, atomically clean substrates are required. This can be achieved by performing experiments in ultra high vacuum ($p < 10^{-9}$ Torr), where surfaces remain clean from residual gases for sufficiently long times. Well defined surfaces are also needed to allow reproducible experiments, which is why single crystal surfaces have extensively been studied. Since materials used in practical applications are far from single crystal surfaces, the results are not directly transferable to the macroscopic world. Much attention has been directed to more complex model systems than pure single crystals, such as model catalysts of clusters on oxides [1].

In this work two model systems have been created by vacuum deposition of metals onto single crystal substrates. Chromium has been deposited onto a thin alumina film created on a NiAl(110) substrate and subsequently oxidized to create a chromium oxide model catalyst. This model catalyst has been characterized with X-ray photoelectron spectroscopy (XPS). Cobalt has been evaporated onto a Cu(001) single crystal to study the initial growth of this system, which shows interesting magnetic properties. The formed structures have been characterized with low energy electron diffraction intensity/energy analysis (LEED I(E)).

Alumina supported chromium oxides are important catalysts in reactions such as selective reduction of nitrogen oxides and dehydrogenation of alkanes. The activity of the chromium oxide catalysts in dehydrogenation has generally been attributed to coordinatively unsaturated Cr^{3+} ions [2, 3]. There can be at least

three kinds of Cr^{3+} ions on the surface: crystalline chromia, redox Cr^{3+} formed in reducing the sample, and non-redox Cr^{3+}, which is present in both oxidized and reduced samples. Which of these are the active species, and how they are related to catalyst structure, is still under debate. The reaction paths in alkane dehydrogenation remain somewhat unclear as well. In this work the model catalyst approach has been used to gain information on the structure and properties of supported chromium oxide catalysts. The object has also been to create a proper model catalyst for study of e.g. dehydrogenation reactions.

Industrial catalyst support materials, such as alumina, are porous and insulating. For surface science studies these are often quite limiting properties, since many spectroscopies require conducting samples and adsorption studies are ill defined without ordered surfaces. We have constructed a model catalyst by evaporating chromium on a thin alumina film created on a NiAl(110) single crystal. This model alumina support has been extensively studied [4–7] and shown to be sufficiently thin for the sample to remain conducting. The film also has an ordered structure that resembles the alumina support used in commercial catalysts.

In order to understand the structures formed on supported catalysts the growth of chromium on the above mentioned thin alumina film has been studied in Publications I and II. To characterize the oxide formed on the model catalyst the interaction of the grown layers with oxygen has also been considered.

To ensure that a proper model system can be created, the model catalyst has been compared to supported catalysts. Chromium oxide catalysts are commonly manufactured by impregnation. Another possible method is atomic layer deposition (ALD), which has been shown to produce active catalysts for e.g. alkane dehydrogenation [2, 8]. The oxidation/reduction behavior of impregnated and ALD catalysts has been studied in Publications III-IV and compared to that of the model catalyst.

Unlike noble metal catalysts, the active species of chromium catalysts are always present in oxide form and the ability to characterize the oxidation state becomes important. In this work, X-ray photoelectron spectroscopy (XPS) has been used to study chromium oxide catalysts, because of the ability of this method to identify the chemical state of the active metal ion. XPS is also non destructive and surface sensitive making it a very useful characterization tool.

The photoelectron spectra of transition metals and their oxides are complex because of several intrinsic and extrinsic poorly known electron energy loss processes. These processes produce a high background, which should be correctly taken into account in the analysis. In Publication V we have studied the effect of different background subtraction methods on the derived chemical state proportions of iron and chromium oxides with more than one oxidation state.

In Publication VI the initial growth of Co on Cu(001) has been characterized with low energy electron diffraction intensity/energy analysis. This system exhibits interesting magnetic properties, such as giant magnetoresistance [9] and magnetic anisotropy [10]. For possible applications, such as spin valves, epitaxial sandwich structures of Cu and Co are usually grown. Undesired mixing of the Co/Cu interface has been observed, which has an effect on the magnetic properties. The structure model obtained from the LEED I(E) analysis can be utilized in theoretical studies of the magnetic properties of this system.

Chapter 2

X-ray photoelectron spectroscopy (XPS)

2.1 Features of transition metal core level spectra

X-ray photoelectron spectroscopy (XPS) is one of the most widely used surface characterization methods. Its inherent sensitivity to the chemical state of surface region atoms and its relatively simple use have made it a regular analysis tool.

In XPS the surface is exposed to X-rays, which through the photoelectric effect produce electrons that leave the sample at a certain kinetic energy. From the measured kinetic energy E_K the binding energy of the electron E_B can be obtained as

$$E_B = \hbar\omega - E_K - \phi_S, \tag{2.1}$$

where $\hbar\omega$ is the X-ray photon energy and ϕ_S the spectrometer work function. The sample work function does not affect the measured binding energy as long as the Fermi levels of the sample and spectrometer are the same. This is not the case for insulating or charged samples, for which an unknown shift in the binding energy occurs. The shift has to be corrected with some common reference point with a known energy, which can cause uncertainty in the peak positions.

Although the penetration depth of e.g. 1486.6 eV AlK_α radiation is of the order of one micrometer, the inelastic scattering of electrons traveling in the sample limits the sampling depth to tens of ångströms making XPS a surface sensitive method. The chemical sensitivity is due to the fact that binding energies are specific for each element and that changes in the chemical state, such as oxidation, cause observable energy shifts. Although chemical bonding occurs by the valence electrons, these chemical shifts are also observed in core levels, which have a far

more intense photoelectron signal. For first row transition metals emission from the spin–orbit split 2p core level is the most intense and is commonly used for analysis.

In addition to the photoelectrons, also Auger electrons are observed in XPS spectra. The Auger transition can roughly be described by a process, where the core hole produced by photoemission is filled with an electron from a higher core level and the released energy is transmitted to another electron, which is emitted. The emitted electrons have element specific kinetic energies and they can also be used for spectroscopic purposes. In Auger electron spectroscopy (AES) the surface is bombarded with a keV electron beam and the kinetic energy of emitted electrons is measured. On top of a secondary electron background Auger peaks are observed. The effects of changes in the chemical state to Auger spectra are not as well known as in XPS and therefore AES is mostly used to measure elemental composition.

The spectral lines of Eq. (2.1) are observed as peaks because of several broadening effects. The inherent Lorentzian line width of a core level is inversely proportional to the lifetime of the created core hole. For the photoelectron spectra of the two 2p core levels of transition metals this can lead to different peak widths via the Coster–Kronig process [11]. In this Auger process the core hole produced in the $2p_{1/2}$ level is filled with an electron from the $2p_{3/2}$ level drastically shortening the lifetime of the $2p_{1/2}$ core hole. Because of its shorter lifetime, the linewidth of the $2p_{1/2}$ peak can be considerably larger than that of the $2p_{3/2}$ level. The finite resolution of the spectrometer and coupling of the core hole to phonons cause additional Gaussian broadening.

Because of several extrinsic and intrinsic electron energy loss processes available for 2p levels of transition metals, the background step for these core levels is very high and the peaks appear to be asymmetric. The extrinsic energy losses are related to inelastic scattering of electrons in a solid whereas intrinsic processes occur during photoionization as a response to the created core hole. The intrinsic losses can extend to kinetic energies of even 50 eV below the main peak. The inelastic background produced by the extrinsic losses extends much further because of multiple scattering.

The core hole created by photoemission causes substantial reorganization, or relaxation, of valence electrons, which can lead to an exited final state in which a valence electron is promoted to a higher unfilled level. This energy will not be available for the photoelectron and this leads to a discrete structure on the low kinetic energy side of the peak. These additional peaks are usually called shake-up satellites.

For metals no discrete shake-up structure is observed, but the continuous distribution of possible states above the Fermi level available for the valence electrons

creates asymmetric broadening on the low kinetic energy side. This results in a lineshape, which has been theoretically described by Doniach and Šunjić (D–S lineshape) [12]. The metals with the highest density of states near the Fermi level exhibit the largest asymmetry. Plasmon losses, which can be either extrinsic or intrinsic, further complicate the spectra.

For transition metal oxides and other inorganic systems very strong satellites can be observed. These are related to strong configuration interaction in the final state involving significant ligand–metal charge transfer instead of pure shake-up processes [13]. Another complication of oxide spectra is the interaction between unpaired core electrons and 3d electrons, which results in multiplet splitting creating a range of possible final states [14]. The energy separation between these states is often so small that discrete peaks do not appear in the spectra, but splitting is observed as asymmetry.

Because of all of the above mentioned processes true quantitative XPS is quite complex despite of the simplicity of Eq. (2.1). In many cases one must resort to peak fitting to derive any chemical information. Before this can be done one must first take into account the so called analyzer intensity/energy response function (IERF) [15], which arises from the energy dependence of the spectrometer performance. Secondly, one has to remove the background created on the low kinetic energy side of the spectrum by inelastically scattered electrons.

A proper background subtraction method should be able to correctly remove the extrinsic energy losses and leave only the intrinsic spectrum. The high step in transition metal spectra makes correct removal of the inelastic background increasingly important. After background subtraction the remaining spectrum is fitted with a synthetic lineshape, which is often approximate, since the intrinsic shape of the spectra arising form all of the different energy loss processes is generally not well known. For quantification of chemical states the use of reference spectra measured from reliable samples can significantly improve the analysis.

Theoretical calculations on e.g. multiplet splitting can yield valuable information on the true intrinsic lineshape. It is also possible to use the theoretical results directly in peak fitting. To obtain a model spectrum the calculated final states should be artificially broadened into a peak envelope to take into account lifetime broadening and the spectrometer resolution. This method is clearly laborious and subject to errors in the model, which makes it inapplicable for routine work. A more convenient way is to use theoretical calculations as a basis for choosing an appropriate synthetic lineshape for peak fitting.

2.2 Background subtraction methods

There are several background subtraction methods available for XPS. The linear and Shirley [16] backgrounds have been widely used because of their relative simplicity. The Shirley background is essentially a scaled integral of the spectrum after background subtraction and is calculated iteratively. The Shirley background correction for a measured spectrum $j(E)$ at kinetic energy E is obtained from

$$F_{k+1}(E) = j(E) - j(E_{min}) \frac{\int_E^{E_{max}} F_k(E')dE'}{\int_{E_{min}}^{E_{max}} F_k(E')dE'}, \tag{2.2}$$

where $F_k(E)$ is the background subtracted spectrum after k iterations and $j(E_{min})$ is the measured intensity at the low kinetic energy endpoint. The calculation converges quite fast and usually only a few iterations are needed. The only parameters required are the endpoints, E_{min} and E_{max}.

The Shirley method is convenient and produces often quite symmetric peaks after background subtraction. However, the Shirley background is an empirical method with no physical justification and is also dependent on endpoint selection.

Tougaard has more recently introduced a background subtraction method that is based on modeling the electron transport in a solid [17]. The Tougaard background correction for a homogeneous bulk sample is calculated as

$$F(E) = j(E) - \lambda \int_E^{\infty} j(E')K(E' - E)dE', \tag{2.3}$$

where λ is the inelastic electron mean free path and $K(E' - E)$ the differential inelastic scattering cross section. Equation (2.3) describes correctly the inelastic energy losses, as long as the true cross section K is known. This is practically never the case and approximations have to be introduced.

Both the cross section K and the inelastic mean free path λ depend on the kinetic energy of the electron, which makes the use of Eq. (2.3) over an large energy range quite difficult. Tougaard has shown that the product λK is only weakly energy dependent and could be approximated with a so-called universal cross section [18]

$$\lambda_i K(E_L) = \frac{BE_L}{\left(C + {E_L}^2\right)^2}, \tag{2.4}$$

where E_L is the energy loss in electron volts and B and C are parameters. Tougaard has shown that for bulk transition metals and their oxides universal values of C=1643 eV^2 and $B\approx$3000 eV^2 can be used. It has been also shown that the universal background applies with reasonable accuracy for a wide scale of other structures as well, if B is used as a fitting parameter [19].

Seah has proposed that the Tougaard parameters can be replaced with two new parameters, the centroid energy of a single loss function $\bar{E}$ and the exponential slope of the background E_1=714.9 eV [20]. The centroid energy varies for each element. These new parameters are related to the Tougaard parameters by

$$C = \left(\frac{2\bar{E}}{\pi}\right)^2 \tag{2.5}$$

and

$$B = 2C \exp\left(-\frac{\bar{E}}{E_1}\right). \tag{2.6}$$

In this description the Tougaard universal values are only one possible combination. The value of C is given by Eq. (2.5), if the centroid energy is known. The bulk B parameter is then fixed according to Eq. (2.6).

Seah has used reflection electron energy loss spectroscopy (REELS) to evaluate the inelastic background for several elements. For elements with no sharp plasmon peaks in the loss spectrum these spectra can be quite well reproduced using the Tougaard background with element specific values of the centroid energy $\bar{E}$ [21]. Although REELS is a direct way to measure the inelastic background, the electrons pass the surface region twice and therefore surface energy losses, like the surface plasmons, can be overestimated.

Neither the Shirley nor the Tougaard method gives absolutely correct intrinsic spectra after background subtraction. The Shirley method removes inconsistently an unknown proportion of extrinsic and intrinsic contributions. The Tougaard method removes the extrinsic component, but becomes approximative with the use of a smooth energy loss cross section, such as the universal cross section. The details in the cross section will, however, be smeared out in the measured spectra due to multiple scattering and convolution with the intrinsic peak width. For this reason, the Tougaard background will be less accurate near the peak, where multiple losses have not occurred. The background shape within the peak area is increasingly important, if the chemical states of a certain element are decomposed from one measured core line. Little attention has been previously given to the effect of the background subtraction method on the relative amounts of different chemical states obtained from peak fitting.

In Publication V we have studied the effect of background choice on the chemical state quantification of iron and chromium mixed oxides. Three background subtraction methods have been compared: (i) the Shirley background, (ii) the Tougaard universal background with the parameter values by Tougaard, and (iii) the Tougaard background with the parameter values by Seah (hereafter referred to as the Seah background).

In Publications I and II standard approaches to peak fitting, mainly a Shirley equivalent background and symmetric peaks, have been used producing some fitting artifacts, such as the binding energies of the Cr 2p satellites. In Publications III–V the peak fitting of the Cr 2p region has been refined to include asymmetric peaks. The absolute amounts of different oxidation states are therefore not comparable between these two approaches.

2.3 Chemical state quantification

The object in analyzing a photoelectron spectrum is often the derivation of the relative amounts of certain chemical states. These chemical states are usually weakly resolved and after the background subtraction the spectrum has to be fitted with synthetic lineshapes. This is the case e.g. for transition metals with different oxidation states. We have used a Gaussian–Lorentzian product function combined with an exponential–constant tail in the peak fitting. This type of function has originally been used to approximate the asymmetric D–S lineshape of metallic states. Similar asymmetry can be seen in oxide spectra mainly due to multiplet splitting. We have found that this function sufficiently explains both metallic and oxide spectra for iron and chromium. The specific parameters depend on the background subtraction method used.

To study the effect of background choice, we have analyzed iron and chromium oxide 2p XP spectra from mixed oxides containing two oxidation states. In both cases a reference spectrum has been measured for one of the oxidation states and the obtained reference parameters have been utilized in the fitting.

Figure 2.1 shows a reference spectrum for Cr^{3+} measured from bulk Cr_2O_3 powder. The spectrum has been fitted after applying the three above mentioned background subtractions. Bulk values have been used for the background parameter C for Tougaard and Seah backgrounds. B parameters have been obtained by fitting to a wide area scan (not shown) and they correspond well to previously reported bulk values. The discrete peaks indicated by the dotted lines are satellite peaks related to the two parent peaks, $2p_{3/2}$ and $2p_{1/2}$. The apparent asymmetry in the main peaks is due to underlying multiplet structure, which is not resolved [22]. The asymmetric shape of these peaks is well explained with the exponential–constant lineshape, as indicated by the low chi-square values.

The fitting parameters obtained from the reference spectra have been utilized in analyzing the Cr 2p spectrum of an oxidized CrO_x ALD catalyst sample supported on aluminum oxide. This sample contains chromium in two main oxidation states: +3 and +6. The relative amounts of Cr^{6+} from the peak fitting with different background subtractions have been compared. Figure 2.2 shows the fitted

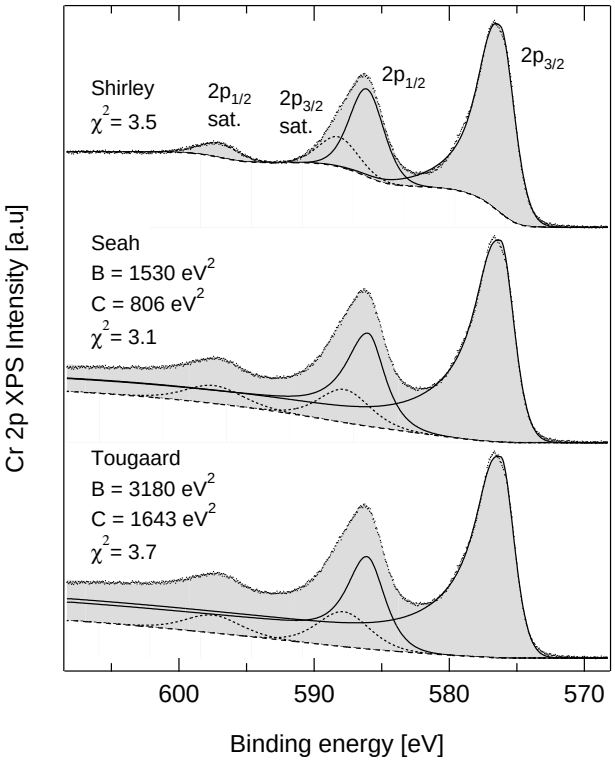

Figure 2.1: Cr 2p XP reference spectrum for Cr_2O_3 (Cr^{3+}) fitted with different background methods. The Shirley background is defined separately for the satellite peak at 598 eV. Tougaard and Seah backgrounds are calculated with bulk like parameters. The shaded area indicates the sum of the component peaks.

spectra for a chemical shift value of 2.8 eV. The B values obtained from fitting Tougaard backgrounds to a separate wide area scan were smaller than bulk values. This was to be expected, since the catalyst contained only 13 wt.% of chromium.

The amounts of Cr^{6+} for a given chemical shift value were found to be within 3 % units for different background subtraction methods. This amount was compared to other typical systematic and random error sources. The uncertainty caused by the choice of background parameters was evaluated to be ± 3 % units. Monte Carlo simulation was used to investigate the random error. Two hundred spectra were simulated by generating random noise to a function fitted to the measured data and subsequently fitting the resulting spectra. This gave a standard deviation of 0.8 % units, which is smaller than the background induced

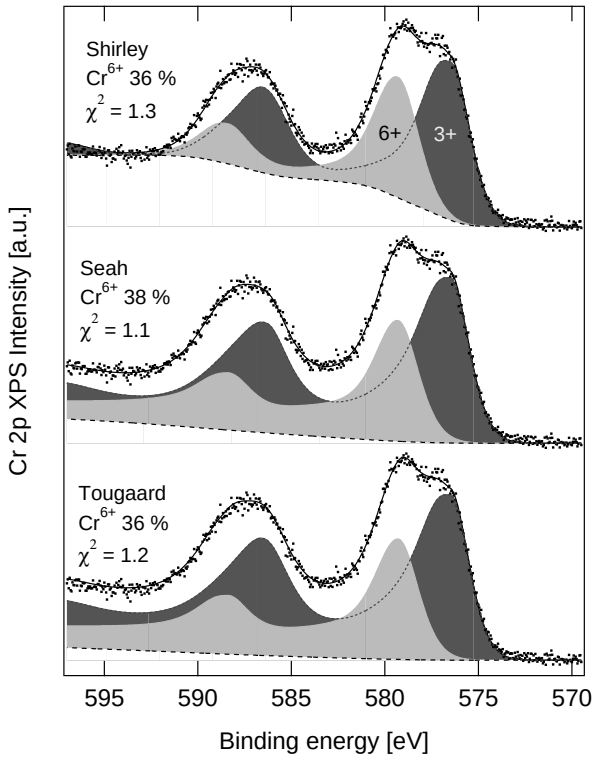

Figure 2.2: Cr 2p spectrum after calcination of an ALD catalyst sample fitted with asymmetric peaks after different background subtractions. Reference fitting values were utilized for Cr^{3+}. The values of B for Tougaard-type backgrounds were evaluated from separate wide scan spectra (not shown). The chemical shift between the two oxidation states was set at 2.8 eV.

error. The dominant systematic error source was found to be the chosen chemical shift between the two chromium oxidation states, the effect of which can be seen in Fig. 2.3. This systematic error was found to be of the same magnitude as the variation caused by different background subtraction methods.

The state for which no reference spectrum was measured, Cr^{6+}, has formally no 3d electrons and hence should not show multiplet splitting. However, it has been shown that for some formally d^0 oxides the net d-electron occupancy can be above zero because of charge transfer from the oxygen sites to the metal sites [23]. Asymmetry was allowed for the Cr^{6+} state in the fitting, but satellite peaks were excluded. The use of symmetric peaks for this state changed only slightly the absolute amounts of Cr^{6+} and did not affect the qualitative observations.

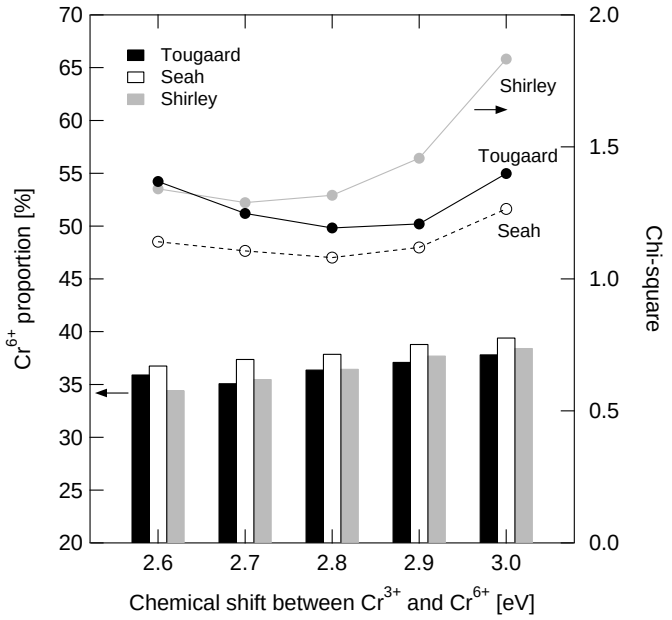

Figure 2.3: The effect of chosen chemical shift between Cr^{3+} and Cr^{6+} on the amount of Cr^{6+}. The background induced error is of the same magnitude as the observed systematic error.

The effect of limiting the analysis to only the $2p_{3/2}$ peak with a Shirley background and using only symmetric peaks was also studied. Without the use of any reference parameters, this standard approach gave totally different values for the amount of Cr^{6+} than the analysis above. It is clear that the use of symmetric peaks without reference spectra can produce misleading values.

A similar analysis as presented for chromium was carried out for bulk Fe_3O_4 after light sputtering to reduce the amount of adventitious carbon. Fe_3O_4 contains iron ions in both +2 and +3 states. A reference spectrum for Fe^{3+} was measured from bulk Fe_2O_3 powder. The amount of Fe^{2+} in Fe_3O_4 was determined after the three background subtractions.

The background induced variation in the proportion of Fe^{2+} was found to be 5–11 % units for a given chemical shift value. The systematic error induced by the chemical shift was at least of the same order or even larger. Another significant systematic error source for iron oxide was found to be the exact reference binding energy. This induced variations of 3-8 % units in amount of Fe^{2+}. The random error was again quite small compared to other error sources, the standard deviation was found to be only 0.5 % units.

In Publication V we have shown that the effect of choice of the background subtraction method in chemical state quantification is comparable to typical systematic errors related to uncertain fitting parameters. Especially in the limit of small concentrations the background choice can even lead to wrong interpretations. Since the true composition of the analyzed samples was in our case unknown, only secondary criteria could be used in evaluating the performance of the different backgrounds. On the basis of these secondary criteria, such as chi-square values and sensitivity to assumptions on peak fitting parameters, the Tougaard background with the parameter values of Seah could be recommended.

Chapter 3

Growth on single crystals

3.1 Thin film growth modes

In ultra high vacuum studies thin film growth is usually carried out by vapor deposition of a desired metal onto the sample. There are several possible growth modes for metallic adsorbates depending strongly on substrate properties. The three most fundamental growth modes are Volmer–Weber 3D growth, intermediate Stranski–Krastanov growth, and Frank–van der Merwe layer-by-layer growth. The basic growth modes are illustrated in Fig. 3.1.

Growth modes can be with some accuracy predicted from surface free energy arguments. If substance B is grown on substance A, then layer-by-layer growth is expected if

$$\gamma_A > \gamma_B + \gamma_{AB}, \tag{3.1}$$

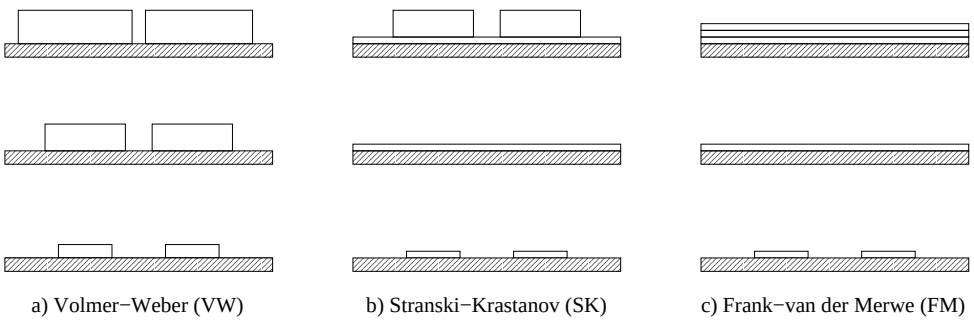

Figure 3.1: The three basic growth modes for thin film growth: a) 3D crystallite growth; b) monolayer followed by crystallites; c) monolayer growth.

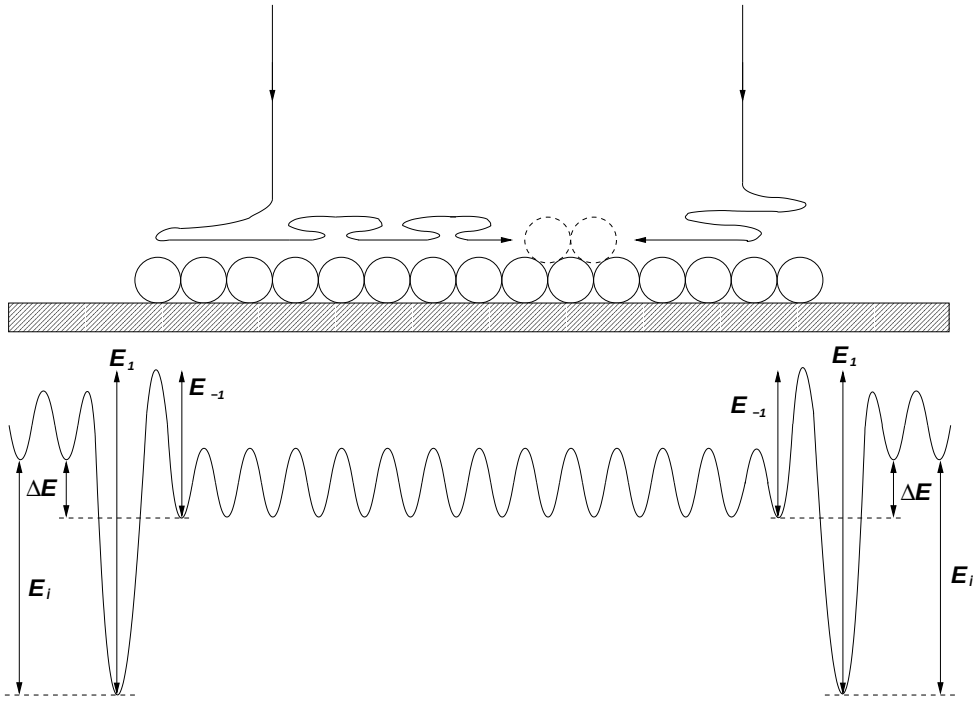

Figure 3.2: Schematic representation of the 2D island growth mode with energy barriers that an adatom experiences when diffusing along the surface.

where γ_A is the surface free energy of substance A in vacuum (and similarly B) and γ_{AB} is the interface free energy. If the condition of Eq. (3.1) is not fulfilled, growth of 3D islands is expected.

Apart from the above three, other possible growth modes include growth of simultaneous multilayers (SM) and monolayer followed by simultaneous multilayer growth (MSM). It is also possible that the substrate and adsorbate phases mix forming surface alloys. Equilibrium growth is not always reached at all temperatures, but several growth modes can be observed with changing substrate temperature.

For metals supported on oxides the equilibrium growth mode is often Volmer–Weber growth, but kinetic limitations have been suggested to lead to formation of 2D islands (2DI mode) [24,25]. In this mode a critical coverage is first reached (15–85 % of a monolayer), after which additional deposited material grows on these islands in a nearly layer-by-layer fashion. The exposed fraction of the oxide then fills up slowly.

This growth mode can be explained by energetics of atom diffusion on the surface. Figure 3.2 shows the energy barriers experienced by an atom diffusing on the surface. The strong attraction to the edge of an island, E_i, arises from lateral metal–metal bonding. The difference between the adsorption energy of the atom on the substrate and on the island, ΔE, is much smaller and positive. The downstepping barrier E_{-1} is also small, but the upstepping barrier E_1, being approximately E_i, is very large. This prevents the islands from reaching their equilibrium 3D shape.

Additional atoms landing on top of the islands can end up in the layer below if the downstepping barrier is thermally accessible. When the islands become larger, atoms diffusing on the islands will encounter each other often enough to nucleate and form new islands. These will attract additional atoms to their edges hindering downstepping. The second layer edges also lower the upstepping barrier from the first layer [25]. In this way the island area growth suddenly slows down and islands begin to thicken. It is obvious that at higher temperature, where uppstepping is facilitated, the growth mode will approach Volmer–Weber 3D growth. The kinetic limitations can, however, lead to the 2DI mode at room temperature and below.

The nucleation described above, which occurs by aggregation of adatoms on regular sites, is termed homogeneous. Nucleation can also be heterogeneous, in which case the adatoms are trapped at defects forming nuclei for subsequent growth.

3.2 Coverage determination

To be able to study thin film growth, we have to know the amount of deposited material. In many cases very small even submonolayer coverages are desired, which makes coverage determination difficult. Quartz crystal microbalance is one of the most used methods giving an absolute measure of the deposited material. Electron spectroscopies, such as AES and XPS, can also be used for coverage determination. When this approach is used, it is inherently assumed that the deposited film consists of full monolayers. The determined coverage is therefore actually the thickness of such a flat film that causes an equal substrate signal attenuation. Since layer-by-layer growth gives the strongest attenuation, the true coverage can be higher.

For AES the attenuation of the substrate signal I_0 by a layer of thickness x is given by

$$I = I_0 \exp\left(-\frac{x}{l_{eff}\cos\alpha}\right), \tag{3.2}$$

where α is the analyzer acceptance angle and l_{eff} the effective attenuation length of electrons at the measured kinetic energy. The exponential behavior is exact for inelastic attenuation, but if elastic scattering is taken into account, this is no longer the case. When using AES with a cylindrical mirror analyzer with its axis normal to the surface, the emission depth distribution function (DDF) is close to exponential and Eq. (3.2) can be used [26]. For XPS the DDF is not exponential, but the same equation can be used if l_{eff} is replaced with an average practical effective attenuation length [27]. Equation (3.2) has been used for film thickness calibration with XPS in Publications I, II and IV. In Publication VI AES has been used for coverage determination using a modified version of Eq. (3.2).

Chapter 4

CrO_x model catalysts

The main focus of the research reported in this dissertation has been on alumina supported chromium oxide catalysts. In them chromium is usually present in two main oxidation states, Cr^{3+} and Cr^{6+}. Some of the Cr^{3+} species can not be oxidized further, which has raised speculations that part of the chromium is incorporated in the alumina lattice. It is generally accepted that the active species on the surface are Cr^{3+} ions, but the structure of the active sites has only been speculated. In Publications I and II chromium growth and oxidation on a thin alumina film has been studied in order to understand the structures formed on supported catalysts.

With controlled oxidation of the chromium layers specific model catalysts can be created to study e.g. the dehydrogenation of alkanes with adsorption and reaction experiments. Palladium supported on Al_2O_3/NiAl(110) has been shown to be active in ethylene hydrogenation [28] suggesting that this model system is suitable for catalytic studies. This NiAl(110) substrate was used also in this work, because the formed thin oxide film is easily reproducible and thin enough to avoid charging in XPS experiments.

4.1 Chromium growth on Al_2O_3/NiAl(110)

The chromium oxide model catalyst was created by vapor deposition of Cr on an oxidized NiAl(110) single crystal. Upon oxidation of NiAl(110) at 550 K a thin well ordered alumina film is formed, which has a structure resembling the commonly used catalyst support material γ-alumina [6]. The thickness of the alumina film is only $\sim$ 5 Å consisting of two bilayers of aluminum and oxygen terminating in an oxygen layer. The alumina film has two domains (A and B),

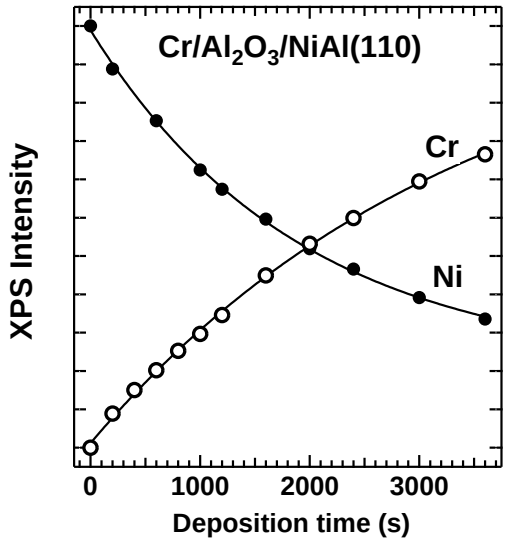

Figure 4.1: XP signal versus time for chromium growth on the model Al_2O_3/NiAl(110) support. The Ni $2p_{3/2}$ intensity represents the attenuation of the substrate signal. The solid lines are exponential curves fitted to the data giving a growth rate of (0.034 ± 0.002) Cr/nm^{2}s.

which are rotated with respect to each other. Several characteristic defects have been clearly identified with STM [29], such as antiphase boundaries (A–A and B–B) probably caused by strain as well as steps and boundaries between domains A and B. Of point defects at least oxygen vacancies are present.

When using thin oxide films as supports it is important to know if the properties of small metal particles on the film are influenced by the underlying metal substrate. If this would be the case, the thin film would not be a good model support. This has previously been studied with various electron spectroscopies. It has been shown that substantial tunneling through the thin oxide layer does not occur on the timescale of the core ionization process and that even on the timescale of the core hole lifetime ($\sim 10^{-15}$ s) charge transfer from the substrate can be disregarded [30]. The charge transfer time is, however, short enough to avoid charging on the surface.

The growth of several other transition metals, such as V, Co, Pt, Rh, Ir and Pd [29, 31–34], on this support has been studied previously. The studied metals show mainly Volmer–Weber (VW) like 3D growth behavior with heterogeneous nucleation at point and line defects. 3D growth of chromium on alumina is also

clearly favored by surface free energy arguments, the surface free energy of Cr single crystals being in the range 2–4 J/m^2 and for Al_2O_3 below 1 J/m^2 [25,35]. However, even if VW growth would be the equilibrium growth mode, kinetic limitations could lead to other modes at room temperature.

Figure 4.1 shows the area of the Ni $2p_{3/2}$ and Cr 2p photoelectron peaks as a function of chromium deposition time for room temperature growth. If the growth would occur in layers, clear breakpoints should be observed in the curve. This is not the case, but smooth near to exponential behavior is observed in stead. Based on this alone, possible growth modes could include the Volmer–Weber mode, growth of simultaneous multilayers (SM) or two-dimensional islands (2DI). Volmer–Weber growth is expected, but the rapid decrease of the substrate signal does not support pure VW mode. Kinetic limitations could lead to the growth of 2D islands at room temperature.

The exponential fits in Fig. 4.1 have been used to derive a nominal growth rate for chromium giving an effective coverage corresponding to a flat layer. Since we did not use any other independent coverage determination method, all reported coverages in this work are nominal. The true coverages are probably somewhat higher, since monolayer growth causes the largest substrate signal attenuation. The determined nominal growth rate was (0.034 ± 0.002) Cr/nm^{2}s. The top layer oxygen density is 12.7 atoms/nm^2 [5], which can be used as a monolayer value for chromium.

Chromium growth has also been studied at 570 K, where the observed substrate signal attenuation was clearly smaller. This could be due to decrease in the initial sticking coefficient or increase in cluster size. If room temperature growth is kinetically limited and equilibrium growth is Volmer–Weber like, then increase of cluster size would be expected.

More detailed analysis of the Cr 2p region in Fig. 4.2 reveals, that a small amount of the deposited chromium is oxidized on the surface. This oxidation must be due to interaction with the oxygen terminated alumina film and could be related to initial heterogeneous nucleation at defect sites, such as oxygen vacancies or steps. Similar initial oxidation on this model support has been observed for e.g. vanadium [32], in which case STM studies also showed that some vanadium atoms were partially incorporated in the alumina film.

A shift towards lower binding energy of the Cr 2p XP peak was observed with increasing chromium coverage. This shift was interpreted to result from an increased proportion of metallic Cr, but it could also be caused by cluster size effects. For small clusters the metallic identity is lost and changes in electronic structure can be expected [29,36]. For these clusters the measured binding energies and line widths of core level spectra can increase compared to that of the

metal. The increase in binding energy is due to the charge left on the cluster in the final state and the broadening arises mainly from the size distribution of the clusters [37]. The transition to a metallic cluster has been estimated to take place in clusters with over 100 atoms, equivalent to cluster diameters around 15 Å. The metallic screening response can, however, be suppressed by the final state charge.

The self energy of the charge on the cluster is the Coulomb energy of a charged conducting sphere, e^2/d, and hence the binding energy shift should scale in the same way with the cluster diameter. This 1/d dependence has been observed for Pd and Rh on the thin alumina film [29]. The observed binding energy shift for chromium could be partly due to this size effect, but the inconsistent shape of the spectra and the fact that fitting is possible with a non-shifting metallic component suggests that they are not dominant in this system.

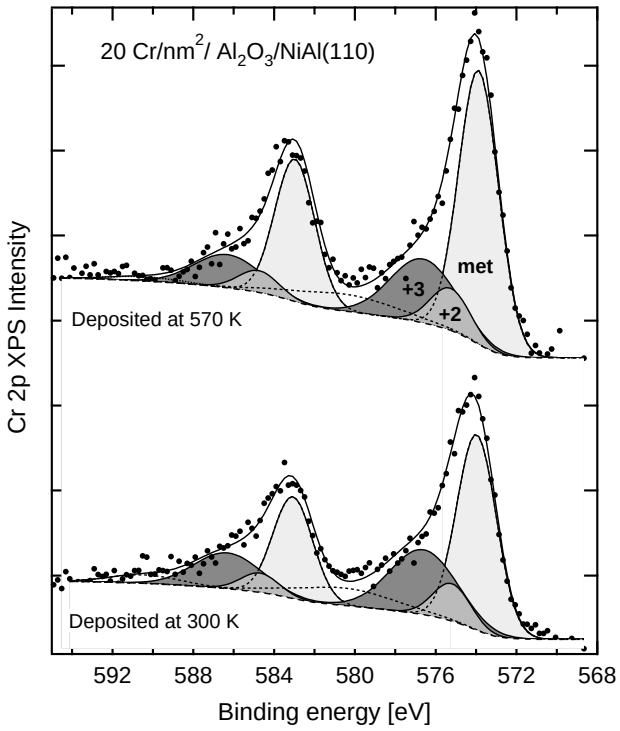

Figure 4.2: Cr 2p XP spectra of chromium deposited at room temperature and at 570 K. The oxidation states are indicated in the figure. Measurements were performed at room temperature.

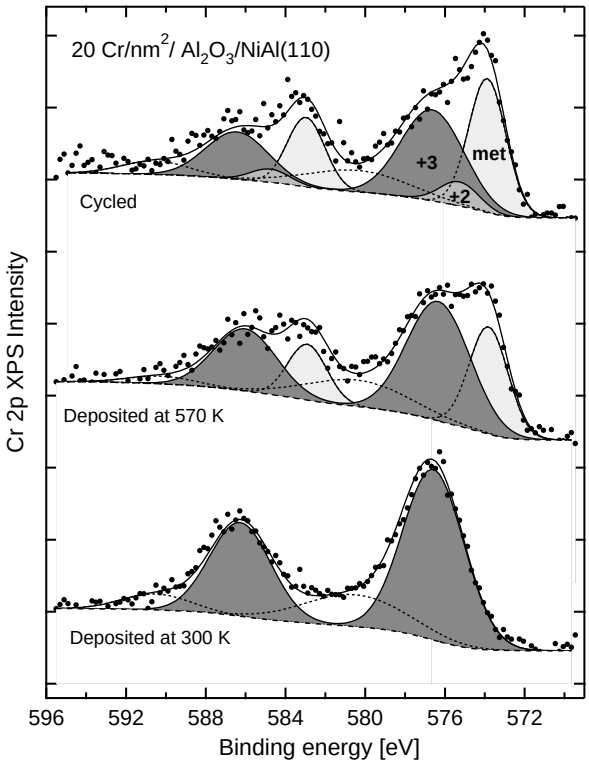

Figure 4.3: Cr 2p XP spectra of oxidized chromium deposited at room temperature and at 570 K. A spectrum for 570 K grown chromium, which has been oxidized, then reduced by heating and reoxidized, is also shown on top (cycled).

4.2 Interaction with oxygen in vacuum

The catalytically active species of many of the previously studies metals on the Al_2O_3/NiAl(110) substrate is metallic, which is not the case for chromium. To create a proper model catalyst we also have to be able to control and characterize the oxidation state of chromium on this substrate. Because of this the interaction of the grown chromium layers with oxygen has been studied.

If the initially mostly metallic chromium layers are exposed to a saturation dose of 20 Langmuirs of oxygen (1 Langmuir = 10^{-6} Torr·s), chromium is readily oxidized. Layers grown at room temperature are totally oxidized to Cr^{3+} up to a nominal coverage of $\sim$ 60 Cr/nm^2 after which some of the chromium remains metallic. For chromium grown at 570 K the oxidation is not total even at lower coverage, as can be seen in Fig. 4.3 for 20 Cr/nm^2.

Room temperature oxidation of Cr(110) leads to an oxidized layer of only about 10 Å [38]. Assuming this for chromium clusters we can state that for 570 K grown chromium the cluster size exceeds 20 Å already in the early stages of growth. This size should also be sufficiently large for the clusters to have a metallic character and therefore the previously observed binding energy shift would be due to initial oxidation of chromium instead of size effects.

If the oxidized layers are heated at 700 K for 5 min, chromium is reduced back to a similar average oxidation state as after deposition. Reoxidation of chromium deposited at room temperature leads to Cr^{3+} as before, but for chromium deposited at 570 K changes are observed upon reoxidation as shown in Fig. 4.3. More metallic chromium is observed indicating that the cluster size is increased upon heating. Since subsequent reduction–oxidation cycles show no changes, an equilibrium cluster shape and size is obviously reached upon heating. Room temperature growth appears indeed to be kinetically limited and Volmer–Weber type 3D growth is probably achieved at 570 K.

If oxidation of chromium was carried out at 700 K, the formed oxide could not be reduced even if heated to 900 K. Temperatures higher than 900 K were avoided since it is known that at high temperature the particles can migrate into the NiAl substrate [39].

When the chromium layers were reduced by heating, no simultaneous oxygen desorption was observed but in stead more oxidized aluminum was found. This effect was confirmed by depositing chromium in an oxygen background pressure of $1.4{\cdot}10^{-6}$ Torr. Figure 4.4 shows Al 2p and Ni 3p spectra before and after this deposition. The Al^{3+} alumina signal is drastically increased upon deposition even though the alumina film should be very inert to additional oxygen. Chromium oxide catalyzes the growth of the alumina film most probably by dissociating oxygen molecules, which can diffuse through the film. This same thickening effect has also been observed for vanadium and palladium [32, 34].

To conclude, the growth and oxidation of chromium on Al_2O_3/NiAl(110) was studied in publications I and II. Room temperature growth was found to be kinetically limited exhibiting smaller and/or flatter clusters than 570 K grown chromium. Oxidation of chromium layers under vacuum led to Cr^{3+} species on the surface. Additional thickening of the alumina film was found to be possible when chromium oxide was present on the surface.

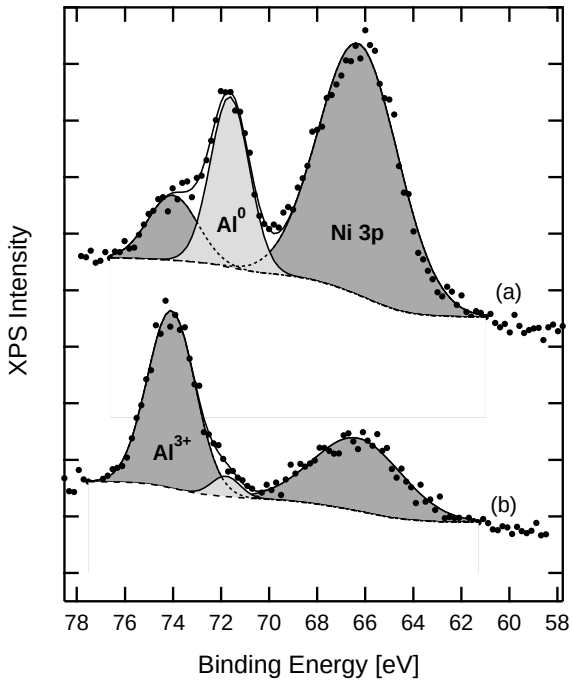

Figure 4.4: Al 2p and Ni 3p XP spectra before (a) and after (b) deposition of 14 Cr/nm^2 in an oxygen background pressure of $1.4{\cdot}10^{-6}$ Torr. The alumina (Al^{3+}) layer has clearly thickened.

4.3 Oxidation state behavior in realistic conditions

To study the behavior of the model catalyst under more realistic reaction conditions the catalyst was transferred in air to another chamber equipped with XPS and a reactor cell allowing treatments at high pressure and temperature. The model catalyst was subjected to normal pretreatments of industrial catalysts, such as calcination and reduction. The calcinations were carried out in laboratory air for 30 min at 850 K and reductions in H_2 (5 % in N_2) for 15 min at the same temperature.

After transfer all chromium was still found to be in the Cr^{3+} state, but additional thickening of the alumina film was observed. The calcination treatment led to formation of previously unseen Cr^{6+}, as shown in Fig. 4.5, even though Cr^{6+} could not be formed on the model catalyst under any vacuum treatment. Simultaneously severe thickening of the alumina film (> 30 Å) was observed. The surface order is most probably lost in this thickening process and new sites for chromium with different oxidation states could be formed. The higher oxygen

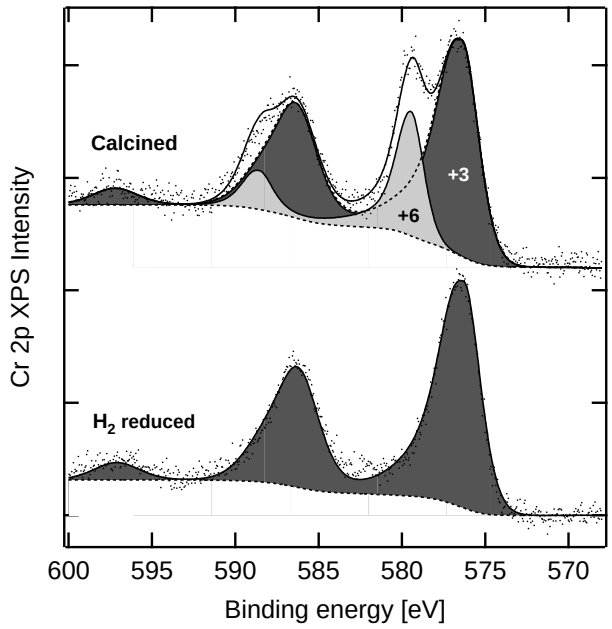

Figure 4.5: Cr 2p XP spectra of the model catalyst with 14 Cr/nm^2 after calcination and after subsequent reduction in H_2. The oxidation states are shown in the figure. Fitting parameters derived in publication V for the ALD chromium oxide catalyst have been used for both oxidation states.

pressure and temperature used in the calcination could also be a requirement for the formation of Cr^{6+}. Another difference to vacuum studies is the introduction of OH-groups on the catalyst when calcining in undried air. OH-groups, which are not inherently found in vacuum, are known to be present on the surface during calcination even at reaction temperatures [40] and can have an effect on the chromium oxidation state.

After calcination the sample was reduced in hydrogen. The hydrogen treatment led to total reduction of Cr^{6+} back to Cr^{3+}, as can be seen in Fig. 4.5. The oxidation/reduction behavior was repeatable, but subsequent cycles were avoided to minimize oxidation of the support.

4.4 Isobutane adsorption

Isobutane dehydrogenation to isobutene is a typical reaction carried out on chromium oxide catalysts. Several models have been suggested for the reaction,

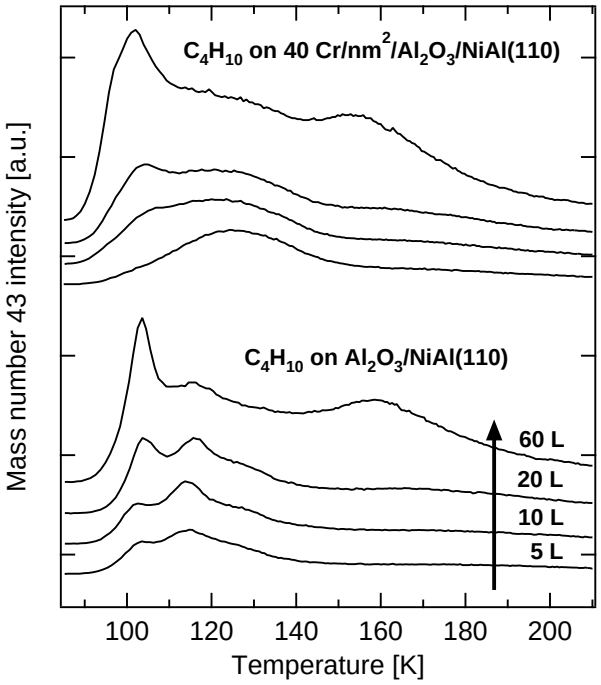

Figure 4.6: Isobutane desorption spectra from the alumina film and from the chromium oxide covered surface as a function of isobutane dose. The peak around 160 K is due to desorption from the surrounding sample holder parts.

including such where dissociative adsorption occurs on a chromium and oxygen ion pair [40]. We have studied the adsorption of isobutane on the model catalyst to gain information on the reaction mechanism and the active sites.

Isobutane adsorption was studied at 70–100 K with XPS and thermal desorption experiments. Adsorption on a thick chromium oxide layer grown at room temperature was compared to adsorption on the thin alumina film formed on the NiAl(110) substrate. XPS measurements on the attenuation of the substrate signal (Ni $2p_{3/2}$) showed that adsorption at temperatures below 90 K led to multilayer formation. The binding energy of the carbon 1s XP peak of adsorbed isobutane was found to be 0.5–1.0 eV lower on chromium oxide covered surfaces than on the alumina film. The change in the binding energy could be interpreted as formation of a chemisorption bond and the direction would support carbon–chromium bonding, rather than bonding to oxygen ions.

Figure 4.6 shows desorption spectra for mass number 43, the main component in isobutane mass spectra, for the chromium oxide covered surface and for the alumina film. Desorption from the multilayer is found around 100 K for both surfaces. For the alumina film monolayer desorption occurs at about 115 K and for the chromium oxide layers at 130 K. The peak at 160 K is due to desorption form the sample holder and should be neglected. The desorption experiments indicate that isobutane is more strongly adsorbed on the chromium oxide layers than on the alumina film. Upon heating up to room temperature all carbon was removed for all of the studied surfaces as indicated by XPS and AES. No hydrocarbons except isobutane were found to desorb from the surface.

Changing the isobutane dose did not affect the positions of the peaks in Fig. 4.6 indicating first order desorption, which is typical for molecular adsorption. Since no carbon was found on the surface after the desorption experiments, it seems that isobutane is molecularly adsorbed on these surfaces. No evidence of dissociation, which would be the requirement for dehydrogenation, was found. Dehydrogenation is usually carried out at high temperatures and pressures and it is possible, that the activation energy for dissociation is too large for it to be observed under these conditions. Another possibility is that the flatter chromium oxide layers formed in room temperature deposition are not active in dehydrogenation. This should be confirmed with additional experiments as a function of the cluster size and shape.

Chapter 5

ALD and impregnated CrO_x catalysts

In the previous chapter properties of a chromium oxide model catalyst were presented. In addition to the model catalyst grown in vacuum, we have studied chromium oxide catalysts prepared by atomic layer deposition (ALD) and impregnation. The reduction of an ALD catalyst has been studied in Publications III and IV. In Publication IV the oxidation state behavior of this catalyst and impregnated catalysts have been compared to the CrO_x/Al_2O_3/NiAl(110) model system using XPS.

5.1 Oxidation and reduction of supported catalysts

In ALD the precursor of the metal oxide is deposited on the support from the gas phase through saturating gas–solid reactions [2]. The metal oxide precursor used was chromium acetylacetonate, $Cr(acac)_3$. Once the alumina support is exposed to $Cr(acac)_3$, a ligand exchange reaction takes place between an acac ligand and OH-groups on the surface. The ligands are then removed e.g. by calcination in air. With ALD more than one adsorption cycle is usually needed to obtain monolayer coverages because of steric effects when using rather large ligands such as acac. Because of the nature of the technique quite good dispersion can be obtained.

The impregnated sample was prepared from $Cr(NO_3)_3{\cdot}9H_2O$. After the impregnation the sample was dried and subsequently calcined. X-ray diffraction measurements indicated that the impregnated sample contained some crystalline Cr_2O_3, but on the ALD sample no crystalline chromia was found.

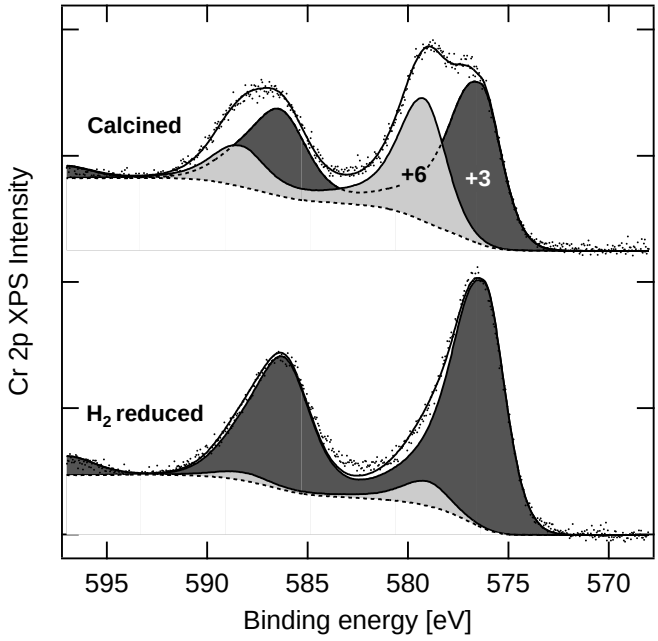

Figure 5.1: Cr 2p XP spectra of an ALD catalyst with 8 Cr/nm^2 after calcination and after subsequent reduction in H_2. The oxidation states are shown in the figure.

When used for dehydrogenation reactions, the supported chromium oxide catalysts are first reduced with e.g. hydrogen or CO. The most noticeable change in the catalysts is the reduction of chromium, but the prereduction of the catalyst with some gases can also lead to unwanted effects like lower activity or increase in side reactions. These are caused by adsorbed species that persist on the catalyst even at reaction temperatures.

To study oxidation and reduction the ALD and impregnated catalysts were calcined in air and reduced in H_2, CO, CH_4 and n-butane. Figure 5.1 shows typical Cr 2p spectra after calcination and reduction for the ALD catalyst. The calcined catalyst contained both Cr^{6+} and Cr^{3+}, much like the model catalyst. Reduction in any of the gases led to almost complete reduction to Cr^{3+}. The impregnated catalyst behaved qualitatively in the same way in terms of oxidation and reduction.

The amount of Cr^{6+} after calcination varied somewhat between samples and different calcinations. Since undried air was used, changes in humidity could have an effect on the oxidation states. For the ALD sample 30–40 % of all chromium

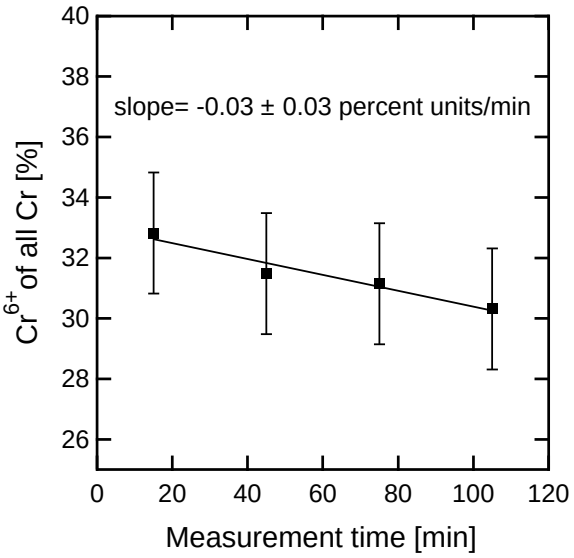

Figure 5.2: The amount of Cr^{6+} in a calcined ALD catalyst as a function of cumulated XPS measurement time.

was found in the Cr^{6+} state after calcination, whereas for the impregnated catalyst the amount was 20–30 %. The calcination of the model catalyst lead to similar results as for the impregnated sample. The differences in the amount of Cr^{6+} could be due to better dispersion of chromium on the catalyst when using ALD [2].

The Cr/Al XPS signal ratio was found to decrease in reductions, which could indicate loss of dispersion, i.e. restructuring of the catalyst material to more crystalline aggregates. This assumption was supported by TPR–Raman measurements. In reduction with CO, CH_4 and n-butane XPS measurements indicated that some carbon was left on the surface after treatments.

The X-ray photoelectric process is know to reduce Cr^{6+} to Cr^{4+} or Cr^{3+} complicating measurements on oxidation states in chromium oxide catalysts [41]. This reduction has been suggested to occur only when hydrocarbons are adsorbed on the sample in e.g. rough pumping. This effect was studied with a calcined ALD catalyst by making repeated measurements and deriving the amount of Cr^{6+} from peak fitting after each measurement. As can be seen in Fig. 5.2 the reducing tendency was indeed observed, but its magnitude was very small, about 0.03 % units per minute, with normal measurements lasting 15 minutes. This amount was found to be insignificant for our interpretations of oxidation states.

In publications III and IV the qualitative oxidation/reduction behavior of the model catalyst was compared to ALD and impregnated catalysts and found to be quite similar. All catalysts were mainly in the Cr^{3+} state after reduction and calcination led to formation of Cr^{6+}. Thus, regarding the chemical state, the model catalyst described in Chapter 4 can be used to study the catalytic behavior of Cr ions of supported catalysts.

Chapter 6

Initial growth of Co on Cu(001)

In Publication VI Auger electron spectroscopy (AES), temperature programmed desorption of CO, and low energy electron diffraction intensity/energy analysis (LEED I(E)) have been used to study the initial growth of Co on Cu(001). Epitaxial sandwich layers of Co and Cu show interesting magnetic properties, but deviation from the desired layer-by-layer growth has been found in the early stages of the growth.

In LEED a low energy beam of electrons is focused on the sample. The electrons with energies in the range 50-500 eV can penetrate only the top few atomic layers of the surface where they are diffracted and observed as spots on a fluorescent screen. In I(E) analysis the intensity of a certain spot is measured as a function of electron energy. These curves are measured for as many LEED spots as possible. The measurements are compared to theoretical curves simulated with quantum mechanical calculations. In Publication VI the symmetrized automated tensor LEED package of Barbieri and Van Hove [42] has been used for calculations.

LEED I(E) analysis involves guessing an initial periodic trial structure for which the theoretical curves are calculated. Comparison between theoretical and experimental I(E) curves is usually made with so called reliability factors (R-factors), of which the Pendry R-factor is the most commonly used [43]. The absolute intensities of I(E) curves are difficult to predict with calculations and accordingly the reliability factors give more weight to correct spectral shape than intensities.

Cobalt is known to grow epitaxially on Cu(001) [44,45], but deviation from layer-by-layer growth is observed for the first few monolayers of Co [46,47]. We found that when ultrathin films of Co were vapor deposited on Cu(001), no additional

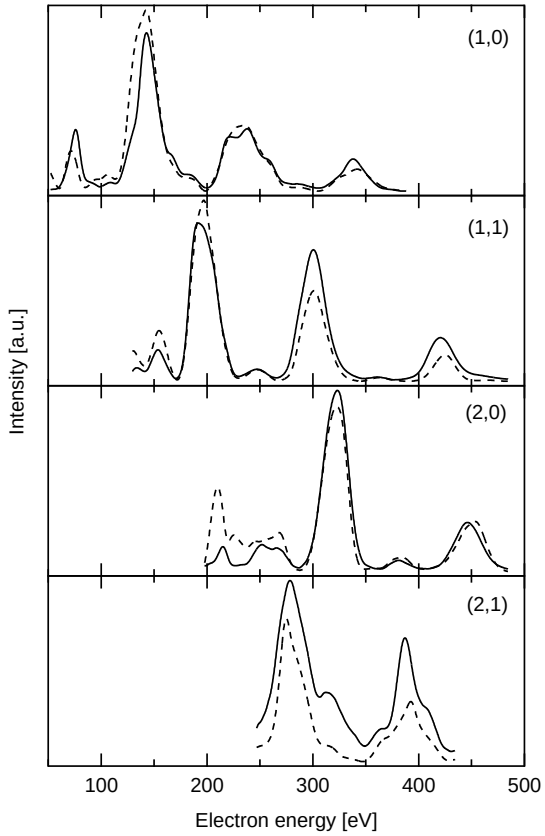

Figure 6.1: Comparison of measured (solid lines) and calculated LEED I(E) curves for the two monolayer nominal Co coverage. The structure used in the calculation is a disordered alloy with 50 % Co in the first and second layers, 100 % Co in the third and 25 % in the fourth layer. The Pendry R-factor is 0.16.

fractional spots were observed in the LEED pattern during the growth indicating that Co forms no ordered structures on the surface other than the 1x1 substrate structure. Because of this only epitaxial layers and substitutionally disordered alloys were considered in the I(E) analysis.

Normally LEED I(E) calculations involve only periodic structures. In order to introduce disorder in the calculations, the averaged t-matrix approximation (ATA) was used [48, 49]. In the ATA scheme disorder is modeled with a periodic structure of pseudo atoms, which have averaged scattering matrices (t-matrices). The result of the calculation is the relative amount of elements within a layer and their average position. In this work the ATA scheme was used to mix the scattering

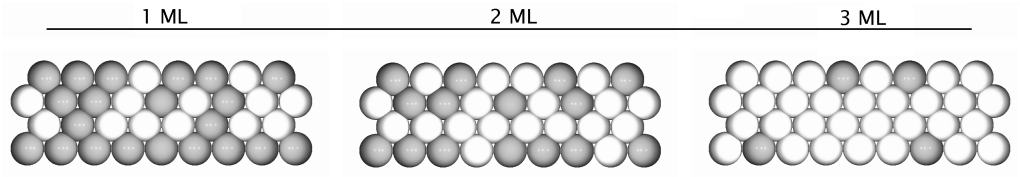

Figure 6.2: Schematic side view of the first four layers during Co growth as obtained from the LEED I(E) analysis. The cobalt atoms (white) take up substitutional copper sites. The deeper layers are pure copper.

properties of Co and Cu in order to model a substitutionally disordered alloy.

To analyze the initial growth, three different coverages of Co were deposited on the Cu(001) surface nominally corresponding to 1, 2 and 3 monolayers of Co. The copper AES signal attenuation was used to identify possible structure candidates using a modified version of Eq. (3.2). Different combinations of epitaxial layers and substitutional alloys were considered.

For the 1- and 2-monolayer cases the I(E) analysis gave the best R-factors for substitutional alloys with 25 to 50 % Co in the first layer. Layer-by-layer growth could be ruled out based on poor R-factors. Fig. 6.1 shows the measured I(E) curves for the 2-monolayer coverage together with the calculated ones for the best fit structure. For the 3-monolayer case the best R-factors were given by structures with mostly cobalt in the top layer indicating a change in the growth mode. In all three cases alloying was observed also in deeper layers than just the first one. A schematic model of the initial growth based on the best fit structures is shown in Fig. 6.2.

To quantify the error in the composition when using ATA, measured I(E) curves for clean Cu(001) were compared to calculated curves with different amounts of Co mixed with the ATA scheme. Since the expected minima is at 0 % Co, we should allow for negative concentrations of Co as well, although this might introduce some unphysical features in the calculation. The total amount of Cu and Co was, however, always kept at 100 %.

The variation in the Pendry R-factor as a function of relative amount of Co is shown in Fig. 6.3 for the first four layers. The normally used error evaluation with the R-factor variance limits is also shown [43]. The variation in the Pendry R-factor is quite small because of similar scattering properties of Cu and Co. This leads to large errors, if the variance limits are used. This independent error analysis shows, that the true deviation from the known amount of 0 % Co is smaller than the variance limit and sufficiently small to justify the use of ATA.

The results of the I(E) analysis were supported by thermal desorption measurements of CO. Figure 6.4 shows CO desorption spectra for all the nominal coverages studied with the I(E) analysis. Included in the figure is also a typical spectrum from an annealed structure. CO does not adsorb on Cu(001) at room temperature, but acts as a probe for surface Co.

Two peaks are observed in the desorption spectra with the higher temperature peak corresponding to the CO desorption temperature on Co(0001) [50]. This peak could be related to desorption from larger islands of cobalt. This is the dominant component in the desorption spectrum form the 3-monolayer structure, indicating that larger areas of Co are found on the surface at this stage of the growth.

The lower temperature peak could be due to desorption from Co atoms forming a surface alloy with Cu. This type of change in binding strength is known as the ligand effect [51]. The formation of Cu–Co bonds in the surface alloy phase

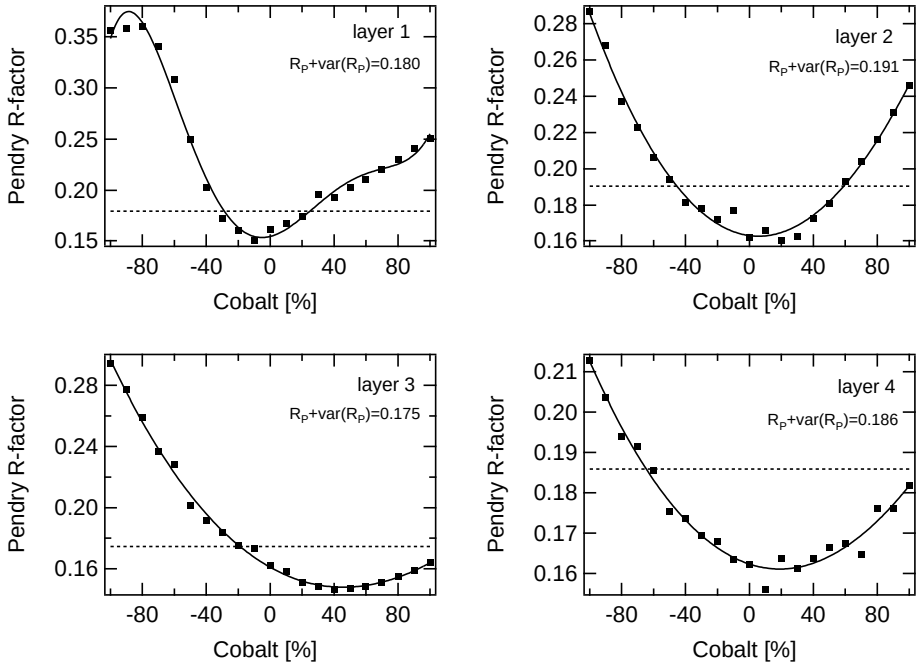

Figure 6.3: ATA error analysis of the Co/Cu(001) system. The best fit Pendry R-factor is shown as a function of Co concentration when compared to spectra measured for clean Cu(001). The R-factor variance limits are shown with dotted lines.

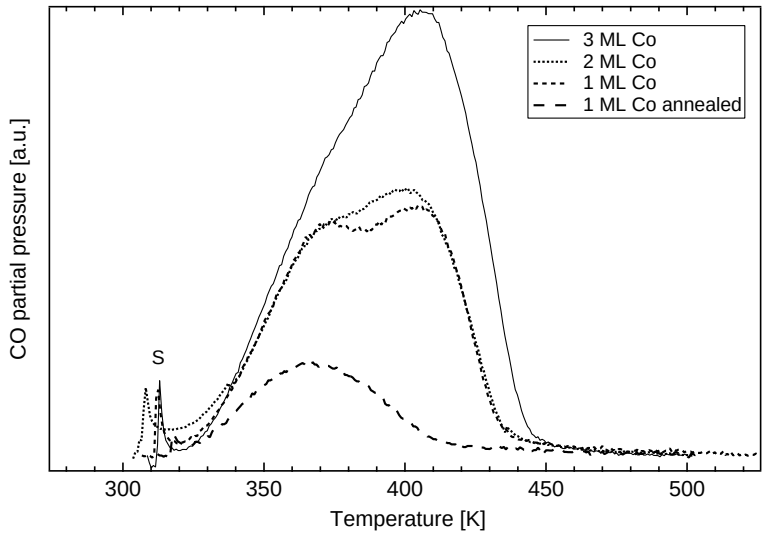

Figure 6.4: CO desorption spectra for different Co coverages on Cu(001). The sharp peaks S are due to desorption from the heating wires.

can change the strength of Co–CO bonding. This type of behavior has been previously observed for many other surface alloys, such as Pt/Sn, Pd/Al and V/Pd [52–54].

After annealing only the lower temperature peak is observed. The annealing is known to induce copper segregation to the surface [55] and hence it seems reasonable that the CO desorption peak from the annealed structure originates form Co atoms forming a surface alloy with Cu.

To conclude, the initial growth of Co on Cu(001) was studied in Publication VI. Both LEED I(E) and CO desorption experiments show that during the growth of the first few monolayers alloying occurs. After this the growth mode starts to resemble layer-by-layer growth. This obtained growth model can be utilized in theoretical studies regarding the magnetic properties of the system as a function of Co film thickness.

Chapter 7

Summary

In this work two model systems have been created by metal evaporation under UHV conditions and characterized by electron spectroscopies. A chromium oxide model catalyst has been studied with X-ray photoelectron spectroscopy. The properties of the model catalyst have been compared to ALD and impregnated chromium oxides used in catalytic applications. Initial growth of a magnetically interesting system, Co on Cu(001), has been studied with low energy electron diffraction. Information on the interface structure is essential to understand the magnetic behavior of the system.

Vapor deposited chromium was initially found to be partially oxidized on the thin alumina film when deposited at room temperature or 570 K. This strong interaction with the substrate could be related to chromium atoms incorporated in the alumina film. At monolayer coverage metallic chromium was easily oxidized to Cr^{3+}, if grown at room temperature. In this way a model catalyst with all the chromium in the active chemical state could be created. 570 K grown chromium layers could not be oxidized totally, which must be due to increased cluster size. Room temperature growth was found to be kinetically limited and possibly exhibits growth of two-dimensional islands.

Chromium oxide on the thin alumina film was also found to catalyze dissociation of oxygen resulting in thickening of the alumina film. This thickening was especially severe when the model catalyst was calcined in air, most probably destroying the ordering of the alumina film. After the calcination previously unseen Cr^{6+} was formed on the model catalyst, much like in supported chromium oxide catalysts. The formation of Cr^{6+} could require high oxygen pressures and temperatures, but could also be related to the changes in alumina structure in calcination.

After calcination both the model and supported catalysts were reducible to Cr^{3+} with e.g. hydrogen treatment. The growth studies under vacuum and XPS measurements on calcined catalysts suggest that the model catalyst structure is closer to impregnated catalysts than ALD catalysts.

The qualitative behavior of the model catalyst and the two supported catalysts was found to be similar in oxidation and reduction despite of the structural differences. This leads us to believe that CrO_x supported on Al_2O_3/NiAl(110) is a relevant model system and can be used to study typical reactions carried out on chromium oxide catalysts, such as alkane dehydrogenation. For this reaction studies under realistic conditions would be needed coupled with e.g. STM studies for structural information.

The possible errors in oxidation state proportions derived from XPS measurements were also characterized. The main focus was on the effect of background subtraction method and this was compared to typical systematic errors induced by uncertainty in peak fitting parameters. For both iron and chromium oxides the background induced variations of ± 5 % and ± 3 % units in the chemical state proportions were found to be comparable to the dominant systematic errors.

Cobalt evaporated onto Cu(001) was found to form random surface alloys during initial growth with Co assuming substitutional copper sites. The results of the LEED I(E) analysis were supported by CO thermal desorption experiments. According to the I(E) analysis these alloys extend to deeper layers than just the first one. With increasing Co coverage a transition to epitaxial layer growth is observed. The obtained structure model can be utilized in theoretical studies of the magnetic properties of this system.

Bibliography

[1] H.-J. Freund, Surf. Sci. **500**, 271 (2002).

[2] A. Kytökivi, J.-P. Jacobs, A. Hakuli, J. Meriläinen, and H. H. Brongersma, J. Catal. **162**, 190 (1996).

[3] F. Cavani, M. Koutyrev, F. Trifiró, A. Bartolini, D. Ghisletti, R. Iezzi, A. Santucci, and G. Del Piero, J. Catal. **158**, 236 (1996).

[4] H. Isern and G. R. Castro, Surf. Sci. **211-212**, 865 (1989).

[5] R. M. Jaeger, H. Kuhlenbeck, H.-J. Freund, M. Wuttig, W. Hoffman, R. Franchy, and H. Ibach, Surf. Sci. **259**, 235 (1991).

[6] J. Libuda, F. Winkelmann, M. Bäumer, H.-J. Freund, T. Bertrams, H. Neddermeyer, and K. Müller, Surf. Sci. **318**, 61 (1994).

[7] M. Klimenkov, S. Nepijko, H. Kuhlenbeck, and H.-J. Freund, Surf. Sci. **385**, 66 (1997).

[8] A. Hakuli, A. Kytökivi, and A. O. I. Krause, Appl. Catal. A **190**, 219 (2000).

[9] G. Binasch, P. Grünberg, F. Saurenbach, and W. Zinn, Phys. Rev. B **39**, 4828 (1989).

[10] S. van Dijken, G. Di Santo, and B. Poelsema, Phys. Rev. B **63**, 104431 (2001).

[11] R. Nyholm, N. Mårtensson, A. Lebugle, and U. Axelsson, J. Phys. F **11**, 1727 (1981).

[12] S. Doniach and M. Šunjić, J. Phys. C **3**, 285 (1970).

[13] A. E. Bocquet, T. Mizokawa, T. Saitoh, H. Namatame, and A. Fujimori, Phys. Rev. B **46**, 3771 (1992).

[14] R. P. Gupta and S. K. Sen, Phys. Rev. B **12**, 15 (1975).

[15] M. P. Seah, J. Electron Spectrosc. Relat. Phen. **71**, 191 (1995).

[16] D. A. Shirley, Phys. Rev. B **5**, 4709 (1972).

[17] S. Tougaard, Surf. Interface Anal. **11**, 453 (1988).

[18] S. Tougaard, Surf. Interface Anal. **25**, 137 (1997).

[19] S. Tougaard, Surf. Sci. **216**, 343 (1989).

[20] M. P. Seah, Surf. Sci. **420**, 285 (1999).

[21] M. P. Seah, I. S. Gilmore, and S. J. Spencer, Surf. Sci. **461**, 1 (2000).

[22] E. Ünveren, E. Kemnitz, S. Hutton, A. Lippitz, and W. E. S. Unger, Surf. Interface Anal. **36**, 92 (2004).

[23] A. E. Bocquet, T. Mizokawa, K. Morikawa, A. Fujimori, S. R. Barman, K. Maiti, D. D. Sarma, Y. Tokura, and M. Onoda, Phys. Rev. B **53**, 1161 (1996).

[24] K. H. Ernst, A. Ludviksson, R. Zhang, J. Yoshihara, and C. T. Campbell, Phys. Rev. B **47**, 13782 (1993).

[25] C. T. Campbell, Surf. Sci. Rep. **27**, 1 (1997).

[26] C. J. Powell, A. Jablonski, I. S. Tilinin, S. Tanuma, and D. R. Penn, J. Electron Spectrosc. Relat. Phen. **98-99**, 1 (1999).

[27] A. Jablonski and C. J. Powell, Surf. Sci. **520**, 78 (2002).

[28] G. Rupprechter, H. Unterhalt, M. Morkel, P. Galletto, L. Hu, and H.-J. Freund, Surf. Sci. **502-503**, 109 (2002).

[29] M. Bäumer and H.-J. Freund, Prog. Surf. Sci. **61**, 127 (1999).

[30] A. Sandell, J. Libuda, P. A. Brühwiler, S. Andersson, M. Bäumer, A. J. Maxwell, N. Mårtensson, and H.-J. Freund, Phys. Rev. B **55**, 7233 (1997).

[31] M. Bäumer, M. Frank, J. Libuda, S. Stempel, and H.-J. Freund, Surf. Sci. **391**, 204 (1997).

[32] M. Bäumer, J. Biener, and R. J. Madix, Surf. Sci. **432**, 189 (1999).

[33] M. Bäumer, M. Frank, M. Heemeier, R. Kühnemuth, S. Stempel, and H.-J. Freund, Surf. Sci. **454-456**, 957 (2000).

[34] S. Shaikhutdinov, M. Heemeier, J. Hoffmann, I. Meusel, B. Richter, M. Bäumer, H. Kuhlenbeck, J. Libuda, H.-J. Freund, R. Oldman, S. D. Jackson, C. Konvicka, M. Schmid, and P. Varga, Surf. Sci. **501**, 270 (2002).

[35] Q. Jiang, H. M. Lu, and M. Zhao, J. Phys.: Condens. Matter **16**, 521 (2004).

[36] M. G. Mason, Phys. Rev. B **27**, 748 (1983).

[37] G. K. Wertheim, S. B. DiCenzo, and D. N. E. Buchanan, Phys. Rev. B **33**, 5384 (1986).

[38] V. Maurice, S. Cadot, and P. Marcus, Surf. Sci. **458**, 195 (2000).

[39] M. Heemeier, S. Stempel, S. K. Shaikhutdinov, J. Libuda, M. Bäumer, R. J. Oldman, S. D. Jackson, and H.-J. Freund, Surf. Sci. **523**, 103 (2003).

[40] S. M. K. Airaksinen, M. E. Harlin, and A. O. I. Krause, Ind. Eng. Chem. Res. **41**, 5619 (2002).

[41] S. V. Kagwade, C. R. Clayton, and G. P. Halada, Surf. Interface Anal. **31**, 442 (2001).

[42] A. Barbieri and M. A. Van Hove, http://www.sitp.lbl.gov/index.php?content=/leedpack/ (2001).

[43] J. B. Pendry, J. Phys. C **13**, 937 (1980).

[44] L. Gonzalez, R. Miranda, M. Salmerón, J. A. Vergés, and F. Ynduráin, Phys. Rev. B **24**, 3245 (1981).

[45] H. Li and B. P. Tonner, Phys. Rev. B **40**, 10241 (1989).

[46] J. Fassbender, R. Allenspach, and U. Dürig, Surf. Sci. **383**, L742 (1997).

[47] F. Nouvertné, U. May, M. Bamming, A. Rampe, U. Korte, G. Güntherodt, R. Pentcheva, and M. Scheffler, Phys. Rev. B **60**, 14382 (1999).

[48] Y. Gauthier, Y. Joly, R. Baudoing, and J. Rundgren, Phys. Rev. B **31**, 6216 (1985).

[49] F. Jona, K. O. Legg, H. D. Shih, D. W. Jepsen, and P. M. Marcus, Phys. Rev. Lett. **40**, 1466 (1978).

[50] J. Lahtinen, J. Vaari, and K. Kauraala, Surf. Sci. **418**, 502 (1998).

[51] W. M. H. Sachtler and R. A. Van Santen, Advan. Catal **26**, 69 (1977).

[52] H. Verbeek and W. M. H. Sachtler, J. Catal **42**, 257 (1976).

[53] V. Matolin, I. Stará, N. Tsud, and V. Johánek, Prog. Surf. Sci. **67**, 167 (2001).

[54] S. Surnev, M. Sock, M. G. Ramsey, F. P. Netzer, B. Klötzer, W. Unterberger, and K. Hayek, Surf. Sci. **511**, 392 (2002).

[55] M. T. Kief and W. F. Egelhoff, Phys. Rev. B **47**, 10785 (1993).